Available online at www.sciencedirect.com
ScienceDirect
Journal of Catalysis 254 (2008) 170–179
JOURNAL OF CATALYSIS
www.elsevier.com/locate/jcat

# Structure and properties of a supported $MoO_3$–SBA-15 catalyst for selective oxidation of propene

T. Ressler [a,*], A. Walter [a], Z.-D. Huang [b], W. Bensch [b]

[a] *Institut für Chemie, Technische Universität Berlin, Strasse des 17 Juni 135, D-10623 Berlin, Germany*
[b] *Institut für Anorganische Chemie, University of Kiel, Olshausenstraße 40-60, D-24098 Kiel, Germany*

Received 26 July 2007; revised 9 October 2007; accepted 13 December 2007

Available online 5 February 2008

**Abstract**

Local structure and catalytic properties of molybdenum oxide supported on nanostructured $SiO_2$ (SBA-15) were studied under reaction conditions by combined X-ray absorption spectroscopy (XAFS) and mass spectrometry. $MoO_3$ supported on SBA-15 exhibits stability and catalytic properties different from those of binary bulk oxides. The interaction between support and molybdenum oxide stabilizes particular hexagonal $MoO_3$ structure that is highly active and selective. The hex-$MoO_3$–SBA-15 is stable under reducing (propene) and oxidizing reaction conditions in the temperature range from 20 to 500 °C. In contrast to bulk hex-$MoO_3$, the onset of activity at about 250 °C is not accompanied by a transformation to $\alpha$-$MoO_3$. Moreover, in contrast to $\alpha$-$MoO_3$, hex-$MoO_3$–SBA-15 is capable of directly oxidizing propene to acrylic acid without additional metal sites.
© 2007 Elsevier Inc. All rights reserved.

*Keywords:* In situ; Heterogeneous catalysis; Structure–activity relationships; EXAFS spectroscopy; X-ray absorption; Molybdenum; Oxides; Hexagonal $MoO_3$; SBA-15; Support; $SiO_2$; Solid-state kinetics

## 1. Introduction

Molybdenum oxides constitute active heterogeneous catalysts for the selective oxidation of light alkenes and alkanes with gas phase oxygen. $\alpha$-$MoO_3$ is the thermodynamic stable binary molybdenum oxide in the temperature range from 20 to 600 °C. However, pure $\alpha$-$MoO_3$ exhibits only moderate catalytic activity, for instance, in the oxidation of propene to acrolein. Moreover, $\alpha$-$MoO_3$ is a rather unselective oxidation catalyst oxidizing propene mostly to $CO_2$ and water. Addition of V or W during preparation of molybdenum oxides results in the formation of mixed oxides (e.g. $(MoVW)_5O_{14}$). The additional metal centers lead to the formation of a variety of characteristic structures. Many of these structures possess open channels such as hexagonal $MoO_3$ (Fig. 1) [1] or pentagonal columns like in $Mo_5O_{14}$ [2] and MoVNbTe oxides [3–5]. The latter exhibits a much higher selectivity compared to $\alpha$-$MoO_3$ [6,7]. Moreover, mixed Mo oxide catalysts are capable of oxidizing propene to acrylic acid which is not observed for $\alpha$-$MoO_3$.

Similar to mixed molybdenum based oxides, binary Mo oxides form a variety of structures different from that of $\alpha$-$MoO_3$ with average Mo valences in the range from 4 to 6. Many of these oxide structures can be readily prepared from a stoichiometric mixture of $MoO_3$ and $MoO_2$ at elevated temperatures (e.g. by chemical vapor transport). However, similar to $\alpha$-$MoO_3$, the onset of reactivity of these various oxides coincides with the onset of bulk oxygen mobility [8,9]. Hence, under reaction conditions in oxygen and alkene at temperatures above 350 °C, most of these oxides rapidly form the more stable $\alpha$-$MoO_3$.

With respect to structure–activity relationships it remains an open question whether additional metal centers in molybdenum oxides (chemical complexity) are inevitable for good activity and high selectivity. Alternatively, a particular structural motif rather than a particular chemical composition may be the prerequisite for high catalytic performance (structural complexity). Answering this question will permit understanding the func-

* Corresponding author. Fax: +49 30 314 21106.
*E-mail address:* thorsten.ressler@tu-berlin.de (T. Ressler).

0021-9517/$ – see front matter © 2007 Elsevier Inc. All rights reserved.
doi:10.1016/j.jcat.2007.12.012

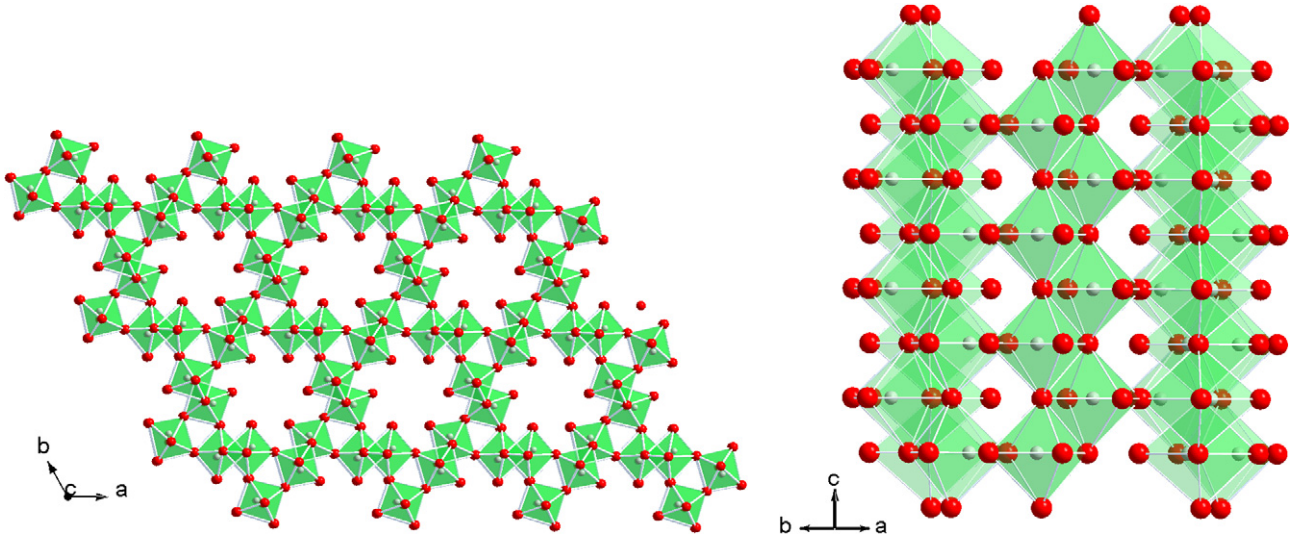


Fig. 1. Schematic representation of the structure of hexagonal $MoO_3$[ICSD 75417] in the *a–b* plane (a) and in *c* direction (b).

tionality of molybdenum based catalysts and developing new and improved catalysts. In order to investigate molybdenum oxides other than $\alpha$-$MoO_3$ under relevant reaction conditions, we have chosen supported molybdenum oxides. Supported oxides offer two advantages for investigating structure–activity relationships. First, interaction with the support may stabilize particular structures which would otherwise decompose into the more stable bulk $\alpha$-$MoO_3$. Second, suitable interaction of the Mo oxide with the support may result in a high dispersion and an improved surface to bulk ratio. Therefore, structural data that relate a particular structure of a catalyst under reaction conditions to its catalytic performance will be more reliable when determined for a catalytic material that possesses a high surface area.

Suitable support materials, in particular for catalyst model systems, should possess a large surface area and a homogeneous internal structure with reasonably large pores. In addition, the support should enable moderate interaction with the oxide catalyst but should be inactive in the oxidation of alkenes. Nanostructured $SiO_2$ materials such as SBA-15 [10,11] constitute suitable support systems for oxide catalysts [12–15]. Vanadium oxide supported on SBA-15, for instance, has been suggested to exhibit isolated $VO_4$ species or low dimensional oxides. However, the detailed local structure of the supported oxide under reaction conditions is still being debated. Furthermore, little has been reported on improved catalytic properties of the supported oxides compared to conventional bulk catalysts. Here, we present investigations of the structure and the catalytic performance of molybdenum oxide supported on nanostructured $SiO_2$ for the selective oxidation of propene.

## 2. Experimental

### 2.1. Preparation of hex-$MoO_3$ supported on SBA-15

8 g of poly(ethylene glycol)-block-poly(propylene glycol)-block-poly(ethylene glycol) triblock copolymer (Aldrich, pluronic, P-123) was dissolved in 240 g of water and 28.6 g of concentrated hydrochloric acid at 30 °C on a water bath. After drop wise addition of 16 g of tetraethyl orthosilicate (TEOS), the reaction mixture was stirred for 24 h at 30 °C. The resulting gel was transferred into a Teflon bottle and heated to 80 °C for 24 h to obtain SBA-15 with 6 nm pores. The resulting white powder was filtered and washed with deionized water, and the surfactant was removed by Soxleth extraction at 78 °C with a mixture of 970 mL of ethanol and 30 mL of concentrated hydrochloric acid. After washing with ethanol, the white powder was dried at RT for about one week.

Typically, 1 g of SBA-15 was stirred in aqueous solutions containing ammonium heptamolybdate $(NH_4)_6Mo_7O_{24}{\cdot}4H_2O$ (AHM, 0.09 mol/L) at pH 7–8. After stirring at room temperature for 18 h, the products were filtered without washing. The impregnated SBA-15 was calcined at 500 °C for 3 h in air to obtain $MoO_3$. The Mo loading of the catalysts was 13 wt% and the synthesized products were stored in dried air. Further details on the preparation procedure and structural characterization of the material obtained are provided in Ref. [16]. Commercial $\alpha$-$MoO_3$ (Aldrich) was employed as-is. Hexagonal $MoO_3$ was prepared by precipitation from an aqueous solution of AHM (0.7 mol/L (Mo)) by addition of $HNO_3$ (1 mol/L). The precipitation was conducted at 50 °C and a pH of 1. Subsequently, the sample was aged for 1 h at 35 °C, filtered, and dried in a desiccator [17]. Phase purity and structure of the reference oxides (hex-$MoO_3$, ICSD 75417) were confirmed by X-ray powder diffraction. The three samples investigated here are denoted as follows: bulk orthorhombic $MoO_3$ ($\alpha$-$MoO_3$), bulk hexagonal $MoO_3$ (hex-$MoO_3$), and hexagonal $MoO_3$ supported on SBA-15 (hex-$MoO_3$–SBA-15). Upon activation under reducing or reaction conditions hex-$MoO_3$–SBA-15 exhibits characteristic structural changes. To distinguish between the as-prepared hex-$MoO_3$–SBA-15 and the material under reaction conditions, the activated sample is denoted as $MoO_x$–SBA-15.

### 2.2. X-ray absorption spectroscopy (XAS)

In situ transmission XAS experiments were performed at the Mo K-edge (19.999 keV) at beamline X1 at the *Hamburg Synchrotron Radiation Laboratory*, HASYLAB, using a Si(311) double crystal monochromator (measuring time ∼4 min/scan). The storage ring operated at 4.4 GeV with injection currents of 150 mA. The in situ experiments were conducted in a flow-reactor at atmospheric pressure in flowing reactants (1 vol% propene in He, 5 vol% oxygen in He, total flow ∼30 mL/min, temperature range from 25 to 500 °C, heating rate 4 K/min). The gas phase composition at the cell outlet was continuously monitored using a non-calibrated mass spectrometer in a multiple ion detection mode (QMS200 from *Pfeiffer*). The mass spectrometer was used for its suitable time resolution. Because Faraday cup and channeltron were employed as detectors, reliable calibration and quantification were not feasible. Hex-$MoO_3$–SBA-15 is introduced as model system. A quantitative comparison to more active or industrial catalysts was not intended. Conversion of propene was estimated from the propene ion current ($m/e$ 42) before and during reaction to be about 10% at 450 °C. Hexagonal $MoO_3$ and $\alpha$-$MoO_3$ were mixed with boron nitride (∼7 mg $MoO_3$, 30 mg BN) and pressed with a force of 1 ton into a 5 mm in diameter pellet resulting in an edge jump at the Mo K-edge of $\Delta\mu_x \sim 1$. Hex-$MoO_3$–SBA-15 was employed as-is. X-ray absorption fine structure (XAFS) analysis was performed using the software package WinXAS v3.1 [18]. Background subtraction and normalization were carried out by fitting linear polynomials to the pre-edge and the post-edge region of an absorption spectrum, respectively. The extended X-ray absorption fine structure (EXAFS) $\chi(k)$ was extracted by using cubic splines to obtain a smooth atomic background, $\mu_0(k)$. The radial distribution function $FT(\chi(k))$ was calculated by Fourier transforming the $k^3$-weighted experimental $\chi(k)$ function, multiplied by a Bessel window, into the $R$ space. EXAFS data analysis was performed using theoretical backscattering phases and amplitudes calculated with the ab initio multiple-scattering code FEFF7 [19]. Single scattering and multiple scattering paths in the hex-$MoO_3$ model structure (ICSD 75417 [1]) were calculated up to 6.0 Å with a lower limit of 4.0% in amplitude with respect to the strongest backscattering path. EXAFS refinements were performed in $R$ space simultaneously to magnitude and imaginary part of a Fourier transformed $k^3$-weighted and $k^1$-weighted experimental $\chi(k)$ using the standard EXAFS formula ($k$ range from 3.4 to 15.1 Å$^{-1}$, $R$ range 0.7 to 4.1 Å) [20]. Structural parameters determined are (i) one $E_0$ shift, (ii) Debye–Waller factors for single-scattering paths, and (iii) distances of single-scattering paths. Coordination numbers (CN) and $S_0^2$ were kept invariant in the refinement.

## 3. Results and discussion

$MoO_3$ supported on SBA-15 was prepared by impregnation of SBA-15 with ammonium heptamolybdate solution followed by calcination in air at 500 °C. Structure and properties of the resulting molybdenum oxide on SBA-15 under reaction conditions was studied by combined X-ray absorption spectroscopy (XAFS) and mass spectrometry. The Mo K near-edge spectra (XANES) and the Fourier transformed XAFS $\chi(k)$ function of hex-$MoO_3$–SBA-15 are compared to those of $\alpha$-$MoO_3$ and bulk hex-$MoO_3$ in Fig. 2. The relative amplitudes of the features in the XANES spectrum of hex-$MoO_3$–SBA-15 resemble more closely that of hex-$MoO_3$ than that of $\alpha$-$MoO_3$ (arrow in Fig. 2). Analysis of the Mo K-edge position yields an average valence of 6. The Fourier transformed XAFS $\chi(k)\cdot k^3$ are not phase shift corrected. Thus, the distances in the $FT(\chi(k)\cdot k^3)$ are shifted by ∼0.4 Å to lower values compared to the crystallographic distances. In the range of Mo–O distances, the $FT(\chi(k)\cdot k^3)$ of hex-$MoO_3$–SBA-15 strongly resembles that

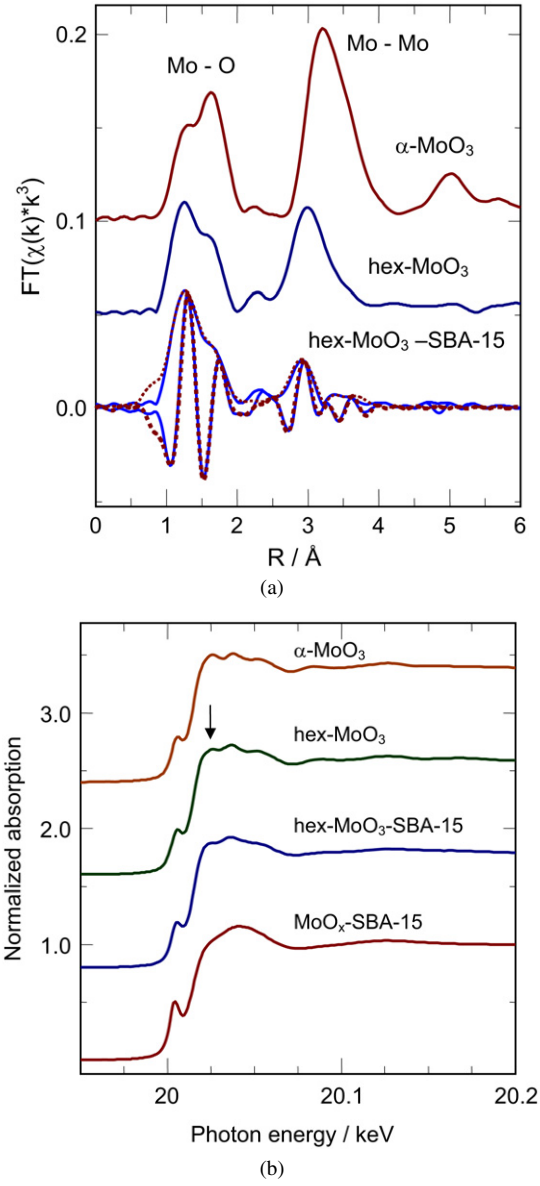


Fig. 2. Experimental Mo K-edge Fourier transformed $\chi(k)$ of hexagonal $MoO_3$, $\alpha$-$MoO_3$, and hex-$MoO_3$–SBA-15 (13 wt% $MoO_3$) together with a theoretical XAFS function (a) and Mo K-edge XANES spectra of $\alpha$-$MoO_3$, hexagonal $MoO_3$, hex-$MoO_3$–SBA-15, and activated $MoO_x$–SBA-15 under reaction conditions (propene + oxygen) (arrow indicates distinct differences in spectra of hex-$MoO_3$ and $\alpha$-$MoO_3$) (b).

Table 1
Type and number ($N$) of atoms at distance $R$ from the Mo atoms in a hex-$MoO_3$ model system compared to experimental distances and XAFS Debye–Waller factors ($\sigma^2$). Experimental parameters were obtained from a refinement of a hex-$MoO_3$ model structure (ICSD 75417) to the experimental Mo K-edge XAFS $\chi(k)$ of hex-$MoO_3$, hex-$MoO_3$–SBA-15 (Fig. 2), and $MoO_x$–SBA-15 under reaction conditions (Fig. 12) ($k$ range from 3 to 14 $Å^{-1}$, $R$ range from 0.9 to 4.1 Å, $E_0$ (hex-$MoO_3$) = −6.5 eV, $E_0$ (hex-$MoO_3$–SBA-15) = −6.6 eV, $E_0$ ($MoO_x$–SBA-15) = −5.9 eV, residual = 6.7, $N_{ind}$ = 25, $N_{free}$ = 17). The uncertainty in the distances and the Debye–Waller factors amounts to about 0.03 Å and 0.0002 $Å^2$, respectively

| Type | $N$ | Model hex-$MoO_3$ | hex-$MoO_3$ | | hex-$MoO_3$–SBA-15 | | Activated $MoO_x$–SBA-15 | |
|---|---|---|---|---|---|---|---|---|
| | | $R$ (Å) | $R$ (Å) | $\sigma^2$ ($Å^2$) | $R$ (Å) | $\sigma^2$ ($Å^2$) | $R$ (Å) | $\sigma^2$ ($Å^2$) |
| Mo–O | 1 | 1.68 | 1.68 | 0.0010 | 1.69 | 0.0058 | 1.67 | 0.0020 |
| Mo–O | 1 | 1.73 | 1.75 | 0.0031 | 1.73 | 0.0019 | 1.69 | 0.0010 |
| Mo–O | 2 | 1.97 | 1.97 | 0.0051 | 1.98 | 0.0035 | 1.90 | 0.0022 |
| Mo–O | 1 | 2.20 | 2.25 | 0.0020 | 2.28 | 0.0033 | 2.32 | 0.0075 |
| Mo–O | 1 | 2.39 | 2.40 | 0.0017 | 2.42 | 0.0078 | 2.36 | 0.0135 |
| Mo–Mo | 2 | 3.31 | 3.33 | 0.0042 | 3.31 | 0.0075 | 3.23 | 0.0142 |
| Mo–Mo | 2 | 3.73 | 3.73 | 0.0035 | 3.79 | 0.0072 | 3.74 | 0.0327 |
| Mo–Mo | 2 | 4.03 | 3.93 | 0.0185 | 3.91 | 0.0221 | 3.94 | 0.0191 |

of hex-$MoO_3$. Structural parameters obtained from a XAFS refinement are given in Table 1. Also in the range of Mo–Mo distances, the $FT(\chi(k)\cdot k^3)$ of hex-$MoO_3$–SBA-15 can be very well described by a hexagonal $MoO_3$ model structure. Apparently, no isolated $MoO_x$ species on $SiO_2$ were detected. The Mo–Mo distance of 3.7 Å in the structure of hexagonal $MoO_3$ corresponds to the distance between corner-sharing $MoO_6$ units (Fig. 1). A particularly increased Debye–Waller factor of this scattering path is obtained for hex-$MoO_3$–SBA-15 compared to bulk hex-$MoO_3$. Hence, the reduced amplitude in the range of the Mo–Mo distances is ascribed to a predominantly two-dimensional hexagonal $MoO_3$ structure supported on SBA-15. Apparently, the two-dimensional hexagonal $MoO_3$ supported on SBA-15 is stabilized by suitable interactions with the support. The lattice parameter $c$ of the hexagonal $MoO_3$ modification is oriented perpendicular to the surface of the $SiO_2$ support (Fig. 1). The increased Debye–Waller factors of the Mo–Mo distance in the $a$–$b$ plane of hex-$MoO_3$–SBA-15 corresponds to an increased static disorder in the $MoO_x$ layer supported on $SiO_2$ compared to bulk hex-$MoO_3$. After thermal treatment a further increase of the Debye–Waller factor indicates a more pronounced two-dimensional hexagonal $MoO_3$ layer structure on SBA-15 under reaction conditions.

### 3.1. Treatment of bulk hex-$MoO_3$ and hex-$MoO_3$–SBA-15 under reducing conditions

Hex-$MoO_3$–SBA-15 exhibited a surprising stability compared to bulk hex-$MoO_3$. Calcination of ammonium heptamolybdate in air results in a temporary formation of hex-$MoO_3$ which rapidly transforms to $\alpha$-$MoO_3$ upon further heating [21]. Conversely, hex-$MoO_3$–SBA-15 is stable at 500 °C in air. Similarly, the reduction behavior of hex-$MoO_3$–SBA-15 differs from that of bulk hex-$MoO_3$. Fig. 3 shows the evolution of Mo K-edge XANES spectra of bulk hex-$MoO_3$ during temperature-programmed reduction (TPR) in propene (20–500 °C, 4 K/min, 1% propene in He). The characteristic XANES spectrum of the resulting oxide at 500 °C indicates that hex-$MoO_3$ is fully reduced to $MoO_2$. The corresponding evolution of the ion current of $H_2O$ ($m/e$ 18), acrolein ($m/e$ 56), and $CO_2$ ($m/e$ 44) during TPR of hex-$MoO_3$ in propene is depicted in Fig. 4. The onset of reduction is at about 350 °C. A detailed discussion of the reduction mechanism and the different profiles of the ion current traces of the oxidation products is beyond the scope of this manuscript and may be presented elsewhere. The clearly separated peaks in the TPR profile are indicative of a multiple step reduction process and the formation of at least two intermediate phases.

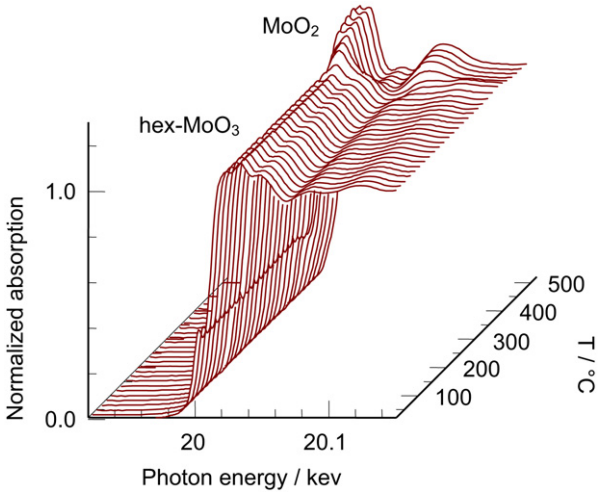


Fig. 3. Evolution of Mo K-edge XANES spectra of hex-$MoO_3$ during temperature-programmed reduction in propene (20–500 °C, 4 K/min, 1% propene in He).

The evolution of the Mo K-edge XAFS $FT(\chi(k)\cdot k^3)$ of hex-$MoO_3$ during TPR in propene is displayed in Fig. 5. Both the XANES spectra shown in Fig. 3 and the $FT(\chi(k)\cdot k^3)$ shown in Fig. 5 exhibit the formation of intermediates in the temperature range from 350 to 400 °C. The $FT(\chi(k)\cdot k^3)$ of the oxide formed above 400 °C is similar to that of $MoO_2$. The distinct changes in amplitude of the $FT(\chi(k)\cdot k^3)$ in the range from 350 to 400 °C indicates the formation of more than one intermediate during reduction of hex-$MoO_3$. Also, a factor analysis of the XANES spectra shown in Fig. 3 yielded four components required to simulate the experimental spectra.

In contrast to the behavior of bulk hex-$MoO_3$ during TPR in propene, hex-$MoO_3$–SBA-15 is not fully reduced to $MoO_2$ during treatment in propene at 500 °C. The evolution of Mo K-edge

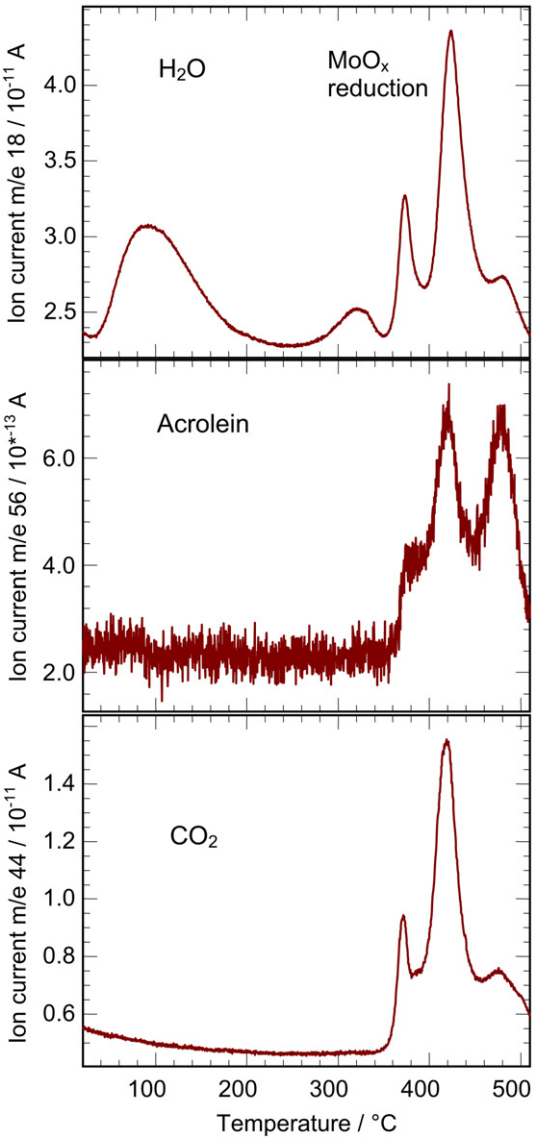


Fig. 4. Evolution of ion current of $H_2O$ ($m/e$ 18), acrolein ($m/e$ 56), and $CO_2$ ($m/e$ 44) during temperature-programmed reduction of hex-$MoO_3$ in propene (20–500 °C, 4 K/min, 1% propene in He).

XANES spectra of hex-$MoO_3$–SBA-15 during temperature-programmed reduction in propene (20–500 °C, 4 K/min, 1% propene in He) is depicted in Fig. 6a. The Mo K-edge XANES of the resulting partially reduced oxide resembles that of $MoO_x$–SBA-15 as depicted in Fig. 2. A slightly increased pre-edge peak and less distinct XANES features are visible in the spectrum of the $MoO_x$–SBA-15 at 400 °C. Both correspond to an increased distortion of the local Mo–O coordination and a disordered two-dimensional hex-$MoO_3$ structure as will be discussed below. Upon heating to 500 °C the pre-edge peak slightly decreased and became less pronounced. Fig. 6b shows the corresponding evolution of the ion currents of $H_2O$ ($m/e$ 18). Compared to the evolution of water during reduction of bulk hex-$MoO_3$ at 400 °C (Fig. 3), very little water evolves during thermal treatment of hex-$MoO_3$–SBA-15. This indicates a lower reducibility and an increased structural stability. The strong interaction between the hexagonal $MoO_3$ and SBA-15

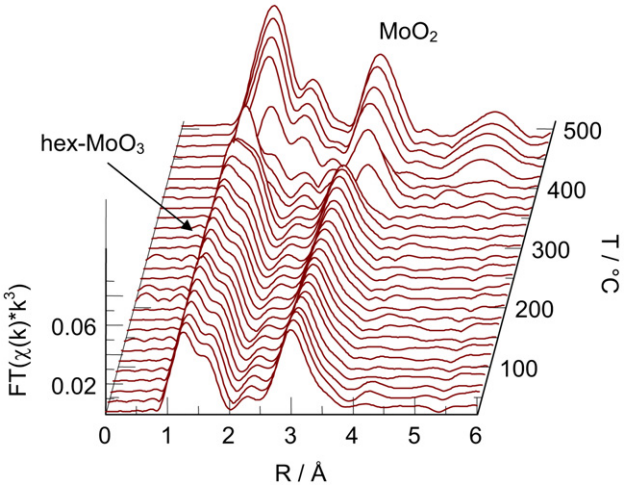


Fig. 5. Evolution of Mo K-edge XAFS $FT(\chi(k)\cdot k^3)$ of hex-$MoO_3$ during temperature-programmed reduction in propene (20–500 °C, 4 K/min, 1% propene in He).

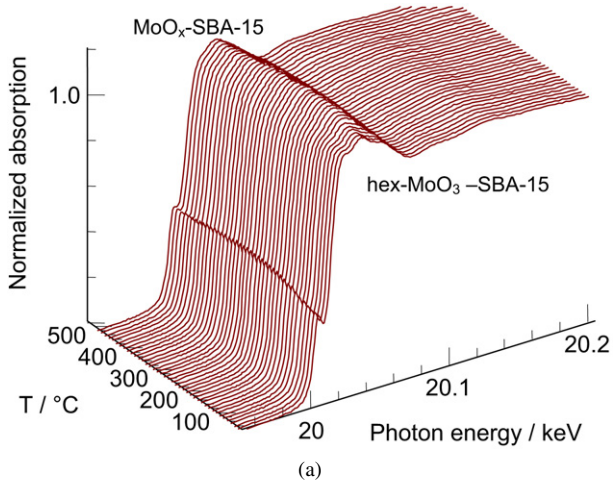


(a)

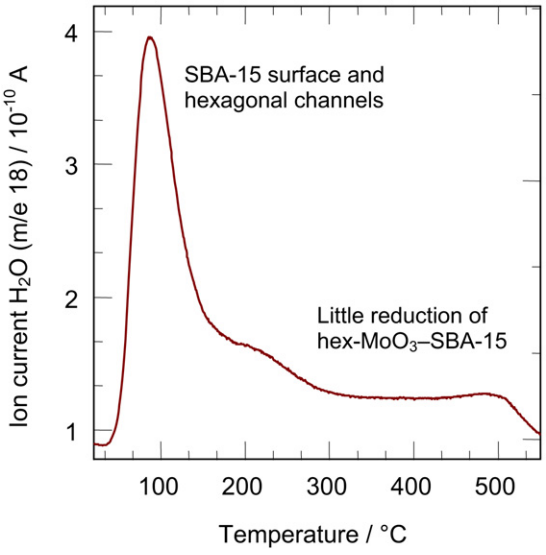


(b)

Fig. 6. Evolution of Mo K-edge XANES spectra (a) of hex-$MoO_3$–SBA-15 during temperature-programmed treatment in propene (20–500 °C, 4 K/min, 1% propene in He) together with (b) the evolution of ion current of $H_2O$ ($m/e$ 18).

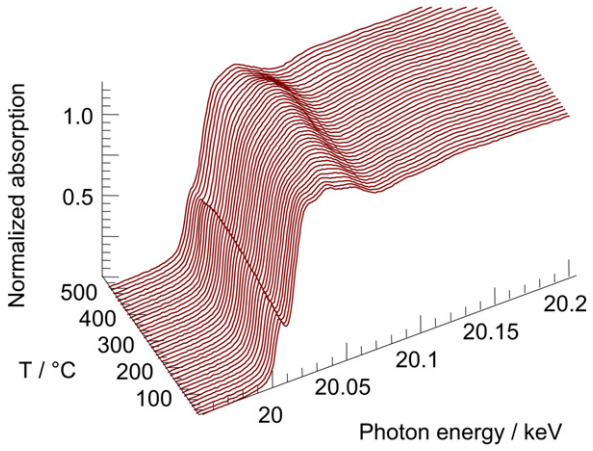


Fig. 7. Evolution of Mo K-edge XANES spectra of hex-$MoO_3$–SBA-15 during temperature-programmed treatment in hydrogen (20–500 °C, 4 K/min, 5% $H_2$ in He).

support that inhibits the formation of $\alpha$-$MoO_3$ under oxidative conditions also prevents the reduction to $MoO_2$ in propene.

In addition to treatment of hex-$MoO_3$–SBA-15 in propene, treatment in 5% hydrogen in helium was studied. The corresponding evolution of Mo K-edge XANES spectra of hex-$MoO_3$–SBA-15 during treatment in hydrogen in the temperature range from 30 to 500 °C is depicted in (Fig. 7). Similar to the treatment in propene, the Mo K-edge spectrum of hex-$MoO_3$–SBA-15 exhibited an increase in pre-edge peak followed by a decrease at temperatures above 450 °C. The resulting phase resembled that obtained after treatment of hex-$MoO_3$–SBA-15 in propene. In contrast to bulk hex-$MoO_3$, hex-$MoO_3$–SBA-15 was stable at 500 °C in hydrogen and did not exhibit further decomposition or reduction to $MoO_2$. Hence, the results of the treatment in hydrogen exclude the formation of carbonaceous deposits being the origin of the low reducibility of hex-$MoO_3$–SBA-15. The low reducibility in hydrogen further corroborates the effect of the interaction between the hexagonal $MoO_3$ and the SBA-15 support on the stability of hex-$MoO_3$–SBA-15.

Apparently, the lattice oxygen of hexagonal $MoO_3$ supported on SBA-15 is not readily available to gaseous reactants. The very low reducibility and the formation of an activated species during treatment in propene is similar to the behavior of polyoxomolybdates (e.g. $H_4[PVMo_{11}O_{40}]$) under reaction conditions [22,23]. Despite this low reducibility, the hex-$MoO_3$–SBA-15 constitutes a better oxidation catalyst than bulk hex-$MoO_3$ and $\alpha$-$MoO_3$. The onset of reduction and oxygen mobility in molybdenum oxides correlates with the onset of catalytic activity. However, the low reducibility of hex-$MoO_3$ on SBA-15 indicates that pronounced oxygen mobility in the bulk may not necessarily be required for good catalytic performance.

In order to further elucidate the stability and catalytic properties of hex-$MoO_3$–SBA-15 under changing reaction conditions, oxygen was added temporarily to the propene feed at 450 °C. Prior to the addition of oxygen, hex-$MoO_3$–SBA-15 was treated in propene at 500 °C for 15 min. This resulted in a slight reduction of the Mo oxide phase as can be seen from the decreased Mo K pre-edge peak (Fig. 8). Subsequently, oxygen was added

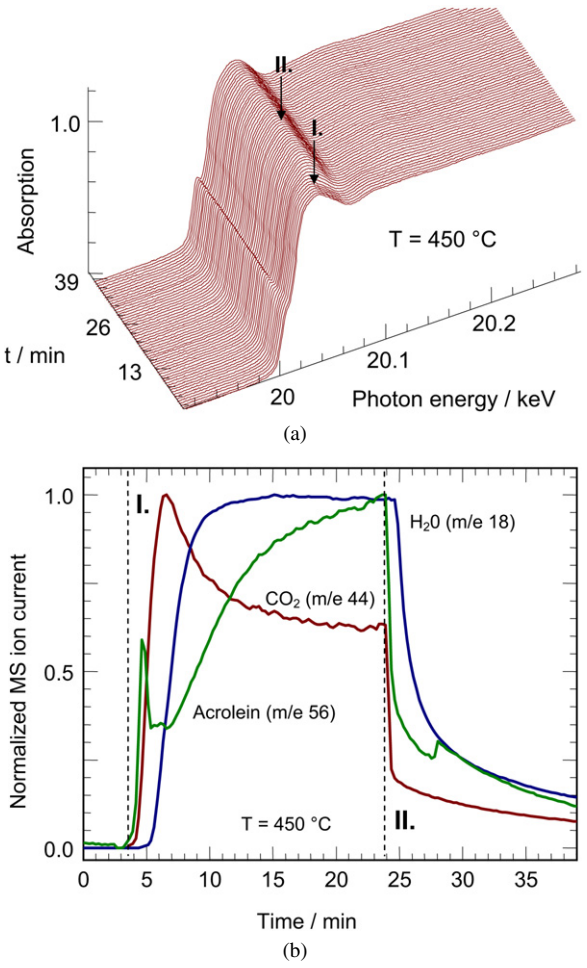


Fig. 8. (a) Evolution of Mo K-edge XANES spectra during isothermal ($T$ = 450 °C) addition of oxygen (5% oxygen in He) during treatment of hex-$MoO_3$–SBA-15 in propene (1% propene in He) (I.—oxygen on; II.—oxygen off). (b) Evolution of normalized ion currents of $H_2O$ ($m/e$ 18), acrolein ($m/e$ 56), and $CO_2$ ($m/e$ 44) obtained by mass spectrometric analysis of the gas phase composition during isothermal addition of oxygen (a). Dashed lines indicate oxygen on (∼3.5 min, I.) or oxygen off (∼24 min, II.).

to the propene feed at 450 °C and switched off again after 20 min. During the isothermal re-oxidation phase (propene + $O_2$ on) and the re-reduction phase (only propene on) Mo K-edge XANES spectra were collected with a time-resolution of 30 s. After the oxidation and reduction treatment, the EXAFS spectrum of the resulting Mo oxide phase supported on SBA-15 was measured. The spectrum and, thus, the local structure of the molybdenum oxide corresponded to that of $MoO_x$–SBA-15 as depicted and discussed in Fig. 12. Hence, the structure of the molybdenum oxide phase supported on SBA-15 after reduction and re-oxidation treatment still corresponded to that of hexagonal $MoO_3$.

The evolution of the XANES spectra and of the MS ion traces of $CO_2$, $H_2O$, and acrolein measured during addition of oxygen to the propene feed at 450 °C are depicted in Fig. 8 (the jump in the $m/e$ 56 signal at ∼5 min was probably caused by a slight change in pressure and sensitivity of the MS). While the concentration of $CO_2$ in the gas phase exhibited a spiked increase, the concentration of acrolein increased more slowly.

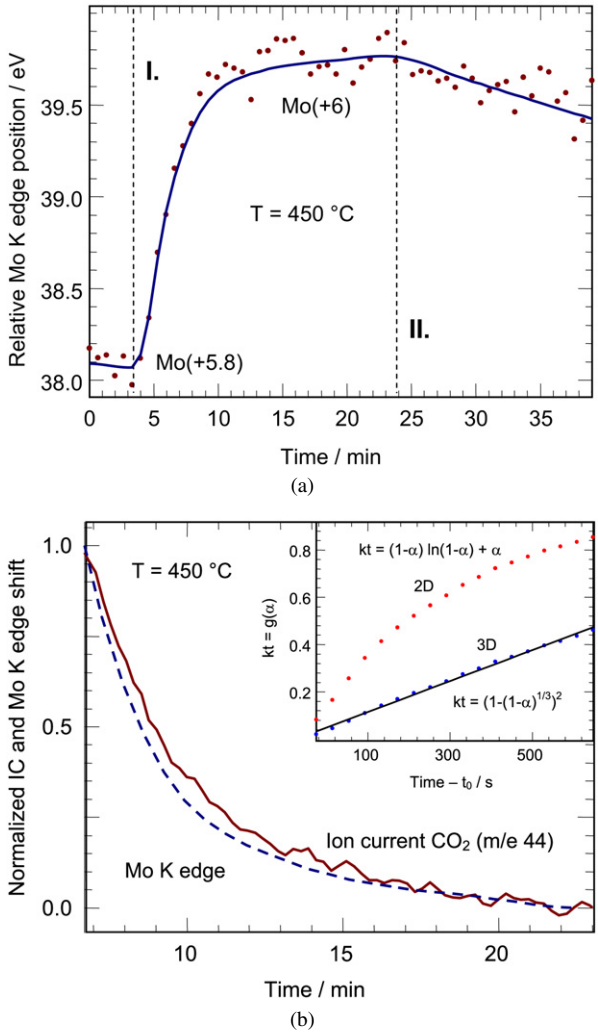


Fig. 9. (a) Evolution of relative Mo K-edge position during isothermal ($T$ = 450 °C) addition of oxygen (5% oxygen in He) during treatment of hex-$MoO_3$–SBA-15 in propene (1% propene in He) (Fig. 8). The average Mo valence in the reduced state (~2 min) and the re-oxidized state (~20 min) is indicated. Dashed lines correspond to addition (~3.5 min, I.) or removal (~24 min, II.) of oxygen. (b) Normalized ion current (IC) of $CO_2$ ($m/e$ 44) together with normalized Mo K-edge position during addition of oxygen (phase I. in Figs. 8 and 9a). The inset shows the integrated function $g(\alpha)$ of the extent of reduction $\alpha$ for a two-dimensional (2D) and three-dimensional (3D) diffusion solid-state kinetic model.

The similar time constants of the increasing acrolein concentration and the decreasing $CO_2$ concentration may correspond to an increasing selectivity during the re-oxidation phase. The evolution of the Mo K-edge position during the oxidation and reduction treatment at 450 °C is depicted in Fig. 9a. The edge position was determined as specified in Ref. [8]. Upon adding oxygen to the propene feed at 450 °C, the Mo K-edge shifted to higher energies indicative of an increased average Mo valence. According to our previously reported calibration curve [8], the molybdenum K-edge positions measured correspond to an average Mo valence of 5.8 after treatment in propene at 500 °C and of ~6.0 after re-oxidation in propene and oxygen (~20 min in Fig. 9a). After switching off the oxygen (II. in Fig. 9a), the Mo K-edge of hex-$MoO_3$–SBA-15 in propene at 450 °C exhibited a slow shift towards lower photon energies. This slow reduction confirms the stability of the hexagonal $MoO_3$ supported on SBA-15. Fig. 9b correlates the re-oxidation rate of the Mo oxide phase in propene and oxygen with the decreasing $CO_2$ concentration in the gas phase (Fig. 8). For comparison, the Mo K-edge shift was inverted and the amplitudes of the two traces were normalized to one. Apparently, the increase in Mo average valence and the decrease in $CO_2$ formation proceed at about the same rate. The inset in Fig. 9b shows the integrated function $g(\alpha)$ of the extent of oxidation $\alpha$ calculated for two solid-state kinetics models (i.e. two-dimensional diffusion or three-dimensional diffusion as rate-limiting step). The inverted and normalized Mo K-edge shift depicted in Fig. 9a was taken as extent of oxidation $\alpha$. The function $g(\alpha)$ is linear with time if the corresponding model is suitable to simulate the experimental data. Solid-state kinetic models tested include one-, two-, or three-dimensional diffusion, various power laws, and Avrami–Erofeev equations [24]. During the first three minutes after adding oxygen to the propene feed the rate of re-oxidation of the Mo is mainly determined by transport of oxygen into the in situ cell. Here, surface or near-surface Mo centers may be rapidly re-oxidized. After three minutes a solid-state kinetic model that assumes three-dimensional diffusion in the Mo oxide bulk to be the rate-limiting step was suited best to simulate the experimental $\alpha$ trace (i.e. Mo K-edge shift) (Fig. 9b). Moreover, Fig. 9b indicates a correlation between the time-dependent change of the average Mo valence and the selectivity of the $MoO_x$–SBA-15 phase under selective oxidation reaction conditions. A similar behavior including rate-limiting three-dimensional diffusion has been reported for activated polyoxomolybdates (i.e. $H_5[PV_2Mo_{10}O_{40}]$) during alternating treatment in propene and propene and oxygen [23]. While a more reduced $MoO_x$–SBA-15 exhibits a decreased selectivity, the selectivity increases with an increasing average Mo valence during re-oxidation of $MoO_x$–SBA-15 in propene and oxygen.

### 3.2. *Treatment of bulk hex-$MoO_3$ and hex-$MoO_3$–SBA-15 under catalytic conditions*

The evolution of the Mo K-edge XAFS $FT(\chi(k)\cdot k^3)$ of bulk hex-$MoO_3$ during thermal treatment under catalytic reaction conditions (1% propene and 5% oxygen in He) is depicted in Fig. 10. The transformation of hex-$MoO_3$ to $\alpha$-$MoO_3$ at about 350 °C is easily detectable. In agreement with the good reducibility of bulk hex-$MoO_3$ in propene, hex-$MoO_3$ readily underwent structural changes under reaction conditions in propene and oxygen. Interestingly, an increase in $FT$ amplitude can be seen prior to the transformation to $\alpha$-$MoO_3$. This behavior was similar to the increase in amplitude at about 350 °C that can be seen in the evolution of the $FT(\chi(k)\cdot k^3)$ of bulk hex-$MoO_3$ during treatment in propene prior to reduction to $MoO_2$. Apparently, an intermediate phase was also formed during treatment under catalytic reaction conditions. The evolution of the MS ion currents of $H_2O$ ($m/e$ 18), acrolein ($m/e$ 56), and $CO_2$ ($m/e$ 44) measured during treatment of hex-$MoO_3$ in propene and oxygen is depicted in Fig. 11. The rapid increase in activity at about 350 °C coincided with the formation of the

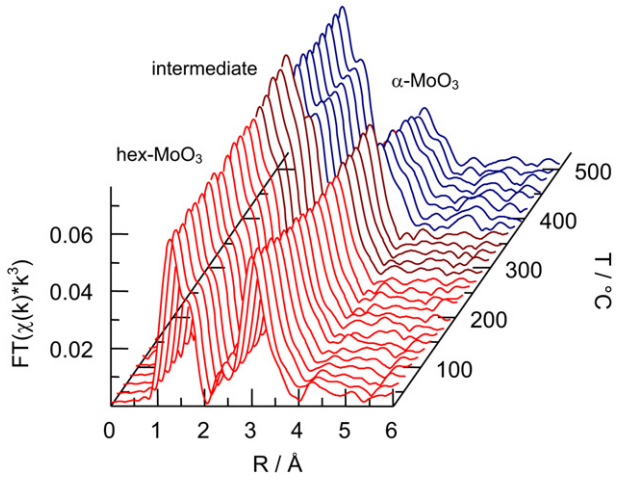


Fig. 10. Evolution of Mo K-edge XAFS $FT(\chi(k)\cdot k^3)$ during thermal treatment of hex-$MoO_3$ in propene and oxygen (20–500 °C, 4 K/min, 1% propene and 5% oxygen in He). The different phases (i.e. hex-$MoO_3$, $\alpha$-$MoO_3$, and an intermediate) are indicated.

intermediate phase. Upon further heating the activity declined corresponding to the transition to $\alpha$-$MoO_3$. No formation of acrylic acid was detected during treatment of hex-$MoO_3$ under catalytic reaction conditions. Hence, the in situ data shown in Figs. 10 and 11 reveal the formation of an intermediate phase with interesting catalytic properties. However, the low stability of this intermediate under reaction conditions did not permit detailed structural characterization and catalytic testing.

While, bulk hex-$MoO_3$ decomposed to $\alpha$-$MoO_3$ at temperatures above 350 °C in propene and oxygen (Fig. 10), hex-$MoO_3$–SBA-15 remained stable up to 500 °C (Fig. 12). During thermal treatment under catalytic reaction conditions the as-prepared hex-$MoO_3$–SBA-15 exhibited only moderate structural changes below 200 °C. After removal of water from the channel structure between 100 and 200 °C (Fig. 6), the $FT(\chi(k)\cdot k^3)$ of the oxide formed remained unchanged up to 500 °C. The corresponding XANES spectrum of activated hex-$MoO_3$–SBA-15 under reaction conditions is shown in Fig. 2 (denoted as $MoO_x$–SBA-15). The increased pre-edge peak is indicative of an increased distortion of the local Mo–O coordination compared to bulk hex-$MoO_3$ and $\alpha$-$MoO_3$. The result of a XAFS refinement of the hexagonal $MoO_3$ model structure (Fig. 1) to the experimental spectrum of $MoO_x$–SBA-15 under reaction conditions is depicted in Fig. 12b. Similar to the spectrum of the as-prepared hex-$MoO_3$–SBA-15, a good agreement between theoretical and experimental spectrum was obtained. The corresponding structural parameters are given in Table 1. Hence, the local structure of $MoO_x$–SBA-15 is also very similar to that of hexagonal $MoO_3$. Again, a majority of isolated $MoO_4$ units on the $SiO_2$ support can be excluded. An increased splitting of the $FT$ peak at about 1.2 Å that corresponds to the first Mo–O coordination sphere can be seen in Fig. 12b. This corroborates the XANES analysis of an increased local distortion of the $MoO_6$ units in activated $MoO_x$–SBA-15. Moreover, the significantly increased Debye–Waller factor of the Mo–Mo scattering path with a distance of 3.7 Å also constitutes a pronounced difference compared to XAFS refinement results of

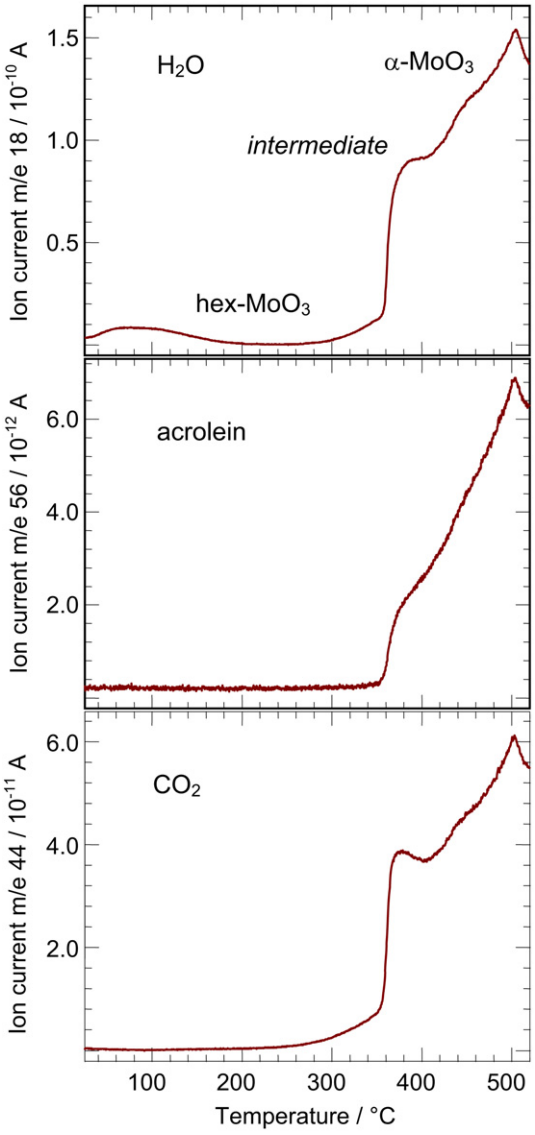


Fig. 11. Evolution of ion currents of $H_2O$ ($m/e$ 18), acrolein ($m/e$ 56), and $CO_2$ ($m/e$ 44) obtained by mass spectrometric analysis of the gas phase composition during thermal treatment of hex-$MoO_3$ in propene and oxygen (Fig. 10) (20–500 °C, 4 K/min, 1% propene and 5% oxygen in He). The different phases (i.e. hex-$MoO_3$, $\alpha$-$MoO_3$, and an intermediate) are indicated.

the as-prepared hex-$MoO_3$–SBA-15. This distance corresponds to the extensions of the channels of hexagonal $MoO_3$ (Fig. 1). The strong decrease of the detectable contribution of this distance to the overall $FT(\chi(k)\cdot k^3)$ indicates a reduced length of the channels and emphasizes a two-dimensional layer structure of hexagonal $MoO_3$ supported on SBA-15.

Apparently, the local structure of the as-prepared hex-$MoO_3$–SBA-15 resembles more closely that of bulk hex-$MoO_3$ than the activated $MoO_x$–SBA-15 (Fig. 2b). The reactivity of the as-prepared hex-$MoO_3$–SBA-15 is strongly modified by interaction with the $SiO_2$ support. This results in the high stability and low reducibility observed (Fig. 6). However, the local structure is dominated by the water still intercalated in the channel structure of the hexagonal modification of $MoO_3$. Upon removal of water (i.e. dehydration) the local structure slightly

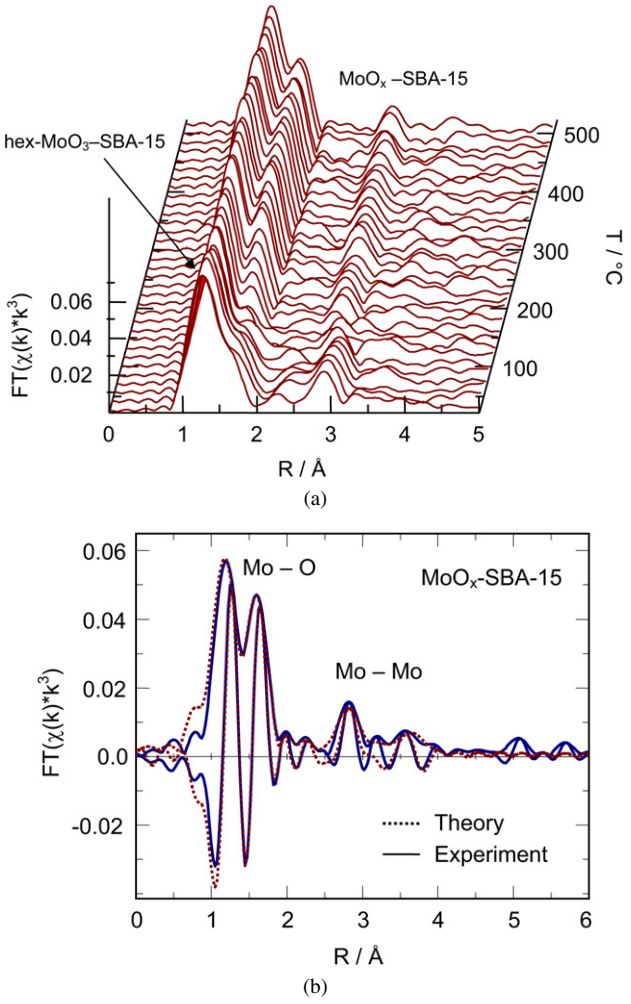


Fig. 12. Evolution of Mo K-edge XAFS $FT(\chi(k)\cdot k^3)$ measured during thermal treatment of hex-$MoO_3$–SBA-15 in propene and oxygen (20–500 °C, 4 K/min, 1% propene and 5% oxygen in He) (a). Experimental and theoretical XAFS function of $MoO_x$–SBA-15 activated in propene and oxygen (b).

rearranges. This may maximize the interaction with the $SiO_2$ support of the characteristic layer structure of the activated $MoO_x$–SBA-15 phase under reaction conditions.

### 3.3. Catalytic performance of hex-$MoO_3$–SBA-15

The MS ion currents of $CO_2$ ($m/e$ 44), acrolein ($m/e$ 56), and acrylic acid ($m/e$ 72) measured during thermal treatment of hex-$MoO_3$–SBA-15 and $\alpha$-$MoO_3$ in propene (1% in He) and oxygen (5% in He) in the temperature range from 20 to 500 °C are depicted in Fig. 13. Apparently, the activated hex-$MoO_3$–SBA-15 catalyst was more active and more selective compared to bulk $\alpha$-$MoO_3$. The onset temperature of activity of $MoO_x$–SBA-15 was shifted to lower temperatures (~250 °C). The ratio of the Mo K-edge jump of hex-$MoO_3$–SBA-15 and $\alpha$-$MoO_3$ amounted to (1:1.6). Normalized to the amount of Mo in the samples, hex-$MoO_3$–SBA-15 was both more active and more selective than $\alpha$-$MoO_3$ (Fig. 13).

Most interestingly, though, hex-$MoO_3$ on SBA-15 was capable of selectively oxidizing propene to acrylic acid (Fig. 13).

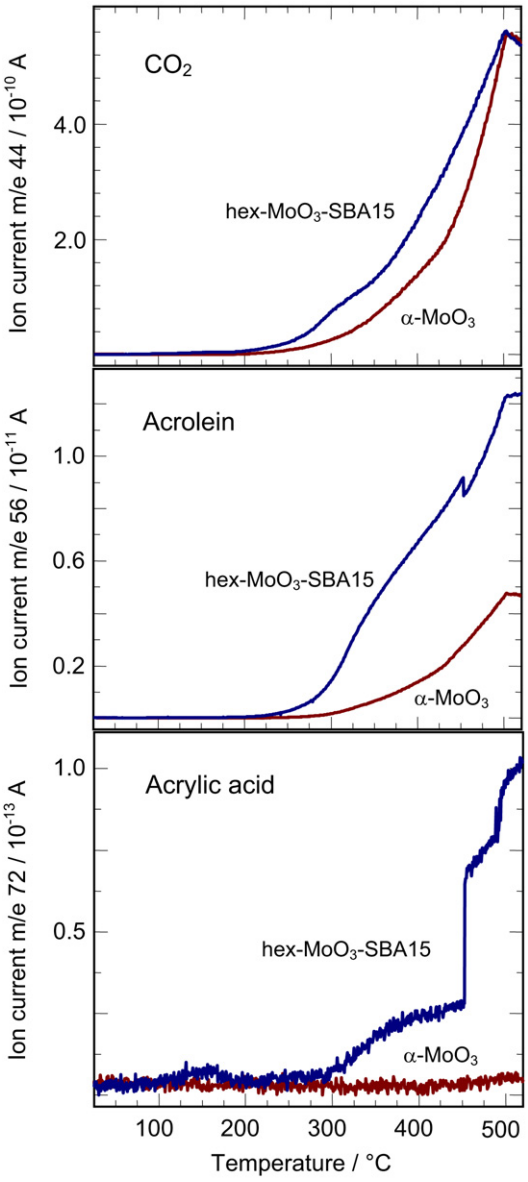


Fig. 13. Evolution of ion currents of $CO_2$ ($m/e$ 44), acrolein ($m/e$ 56), and acrylic acid ($m/e$ 72) obtained by mass spectrometric analysis of the gas phase composition during thermal treatment of hex-$MoO_3$–SBA-15 or $\alpha$-$MoO_3$ in propene and oxygen (20–500 °C, 4 K/min, 1% propene and 5% oxygen in He).

This was not observed during catalytic testing of $\alpha$-$MoO_3$. Binary Mo oxides without additional metal sites were assumed to be incapable of oxidizing propene to acrylic acid. Our data suggest that an increased activity and selectivity is possible without introduction of additional metal centers. The stabilized structure of the hexagonal $MoO_3$ supported on SBA-15 showed not only an increased selectivity but also a new functionality. Therefore, additional metal centers in molybdenum oxide based catalysts are not necessarily required. Evidently, a suitable molybdenum oxide structure alone is capable of activating propene and gas phase oxygen, and selectively oxidizing propene to acrylic acid (Fig. 13). Intriguingly, the stabilized structure of hexagonal $MoO_3$ supported on SBA-15 possesses structural motifs (i.e. an open channel structure) similar to those of the highly active $Mo_5O_{14}$ or "MoVNbTe" catalysts. Hence,

structural complexity of molybdenum oxides is sufficient to improve functional molybdenum sites for the activation of oxygen and alkene followed by selective oxidation of the alkene. Additional metal sites may add functionality and result in further improved catalytic properties. However, adjusting the microstructure of the catalyst (*structural complexity*) may be more important than adjusting chemical composition (*chemical complexity*).

Previous approaches to elucidating structure–activity relationships employing mixed oxide catalysts often simultaneously altered both chemical and structural complexity. This makes it difficult to unravel their individual effects. Hexagonal $MoO_3$ supported on SBA-15 appears to be more suitable to further elucidate the correlations between the structure of molybdenum oxides and the catalytic performance. In particular, the characteristic electronic structure (shape of XANES spectra) of the more active and selective $MoO_x$–SBA-15 under reaction conditions (Fig. 2) could serve as a basis for further theoretically modeling and structural characterization. Once a reliable correlation between structure and properties has been established, further metal centers may be introduced to unravel the effect of additional functional sites on the catalytic performance.

## 4. Conclusions

Supported Mo oxides may exhibit structural and catalytic properties different from those of the corresponding bulk oxides. The interaction between support and molybdenum oxide stabilizes a particular structure that would otherwise not be available for investigations under reaction conditions. Hexagonal $MoO_3$ supported on SBA-15 is more stable than bulk hex-$MoO_3$ and more active and selective in the oxidation of propene to acrolein than the reference $\alpha$-$MoO_3$. Moreover, hex-$MoO_3$–SBA-15 is capable of directly oxidizing propene to acrylic acid without additional metal sites. Thus, the electronic and geometric structure of the Mo oxide under reaction conditions may serve as lead structure for future function property correlations of Mo based oxidation catalysts.

## Acknowledgments

HASYLAB, Hamburg is acknowledged for providing beamtime for this work. We are grateful to A. Hahn and A. Stys for participating in the XAS measurements and to O. Timpe, Fritz-Haber-Institut, Berlin, for providing the hexagonal $MoO_3$ reference sample. The authors acknowledge the German Research Foundation (DFG) for financial support.

## References

[1] J.-D. Guo, P.Yu. Zavalij, M.S. Whittingham, Eur. J. Solid State Inorg. Chem. 31 (1994) 833–842.
[2] L. Kihlborg, Arkiv Kemi 21 (40) (1963) 427–437;
L. Kihlborg, Acta Chem. Scand. 23 (1969) 1834–1835.
[3] M. Hatano, A. Kayou, US patent 5,049,692 (1991).
[4] T. Ushikubo, K. Oshima, A. Kayou, M. Hatano, Stud. Surf. Sci. Catal. 112 (1997) 473–480.
[5] R.K. Grasselli, D.J. Buttrey, P. DeSanto Jr., J.D. Burrington, C.G. Lugmair, A.F. Volpe, T. Weingand, Catal. Today 91–92 (2004) 251–258.
[6] S. Breiter, M. Estenfelder, H.-G. Lintz, A. Tenten, H. Hibst, Appl. Catal. A 134 (1996) 81–89.
[7] O. Ovsitser, Y. Uchida, G. Mestl, G. Weinberg, A. Blume, J. Jäger, M. Dieterle, H. Hibst, R. Schlögl, J. Mol. Catal. A 185 (2002) 291–303.
[8] T. Ressler, R.E. Jentoft, J. Wienold, T. Neisius, J. Catal. 210 (2002) 67–83.
[9] T. Ressler, J. Wienold, R.E. Jentoft, F. Girgsdies, Eur. J. Inorg. Chem. 2 (2003) 301–312.
[10] D.Y. Zhao, Q.S. Huo, J.L. Feng, B.F. Chmelka, G.D. Stucky, J. Am. Chem. Soc. 120 (1998) 6024.
[11] D. Zhao, J. Feng, Q. Huo, N. Melosh, G.H. Fredrickson, B.F. Chmelka, G.D. Stucky, Science 279 (1998) 548.
[12] D.E. Keller, B.M. Weckhuysen, D.C. Koningsberger, J. Phys. Chem. B 110 (29) (2006) 14313.
[13] B.M. Weckhuysen, D.E. Keller, Catal. Today 78 (2003) 25–46.
[14] P. Topka, H. Balcar, J. Rathousky, N. Zilkova, F. Verpoort, J. Cejka, Microporous Mesoporous Mater. 96 (2006) 44–54.
[15] G. Murali Dhara, G. Muthu Kumarana, Manoj Kumara, K.S. Rawata, L.D. Sharmaa, B. David Rajub, K.S. Rama Rao, Catal. Today 99 (2005) 309–314.
[16] Z. Huang, T. Vitoya, D. Deng, H. Modrow, W. Bensch, T. Ressler, J. Mater. Sci. 43 (2008) 244–253.
[17] S. Knobl, Ph.D. thesis, Technical University, Berlin (2004).
[18] T. Ressler, J. Synch. Rad. 5 (1998) 118–122.
[19] J.J. Rehr, C.H. Booth, F. Bridges, S.I. Zabinsky, Phys. Rev. B 49 (1994) 12347–12350.
[20] T. Ressler, S.L. Brock, J. Wong, S.L. Suib, J. Phys. Chem. B 103 (1999) 6407–6420.
[21] J. Wienold, R.E. Jentoft, T. Ressler, Eur. J. Inorg. Chem. 6 (2003) 1058–1071.
[22] T. Ressler, O. Timpe, F. Girgsdies, J. Wienold, T. Neisius, J. Catal. 231 (2005) 279–291.
[23] T. Ressler, O. Timpe, J. Catal. 247 (2007) 231–237.
[24] C.H. Bamford (Ed.), Comprehensive Chemical Kinetics, vol. 2, Elsevier, Amsterdam, 1968.